Energy Conversion and Management 308 (2024) 118394

Contents lists available at ScienceDirect

Energy Conversion and Management

journal homepage: www.elsevier.com/locate/enconman

Assesment for optimal underground seasonal thermal energy storage

J. Gonzalez-Ayala [a,b,*], C. Sáez Blázquez [c], S. Lagüela [c], I. Martín Nieto [c]

[a] Department of Applied Physics, University of Salamanca, Salamanca, Spain
[b] Instituto Universitario de Física Fundamental y Matemáticas (IUFFyM), University of Salamanca, Salamanca, Spain
[c] Department of Cartographic and Land Engineering, University of Salamanca, Higher Polytechnic School of Avila, Avila, Spain

ARTICLE INFO

Keywords:
Energy storage
Geothermal energy
Optimization
Underground 3D map

ABSTRACT

An optimal design for seasonal underground energy storage systems is presented. This study includes the possible use of natural structures at a depth of 100 to 500 m depth. For safety reasons the storage fluid considered is water at an initial temperature of 90 °C. A finite element method simulation using collected data on the thermal properties of the soil was performed. As a practical example of this methodology, an analysis with data collected in the region of Avila, Spain is made. A temperature-depth map using data measured in the zone was generated. A 3D model of the underground material composition was obtained by electromagnetic field diffusion techniques carried out from the surface. This allows for an analysis of available solutions in energy storage strategies, tailored to the specific conditions on the site with a sufficient degree of precision for a first evaluation without the need for deep excavations. This study shows alternating regions of sands and clays, with natural structures for potential use within a depth of 500 m. Thermal properties of water depending on temperature and pressure are considered. A variety of size configurations shows that, in a cylindrical geometry, a storage system with a radius beyond 2 m does not offer significant benefits in energy stored per mass unit. The benefits of a clay envelope are noticeable, compared with the scenario of a cavity surrounded by sand and followed by clay even after 6 months of storage. According to the underground temperature and the energy needed to transport the storage fluid, it is shown that the thermal performance does not significantly improve between 50 m and 100 m of depth. However, between 100 m and 200 m a noticeable improvement is achieved, and from there down to 500 m the improvement is negligible. Several materials for containing the storage fluid and for thermal isolation are analyzed. For periods beyond 14 days, the thermal properties of thermoplastics are relevant, as found in the case of the Acrylonitrile-Styrene-Acrylate which exhibited the best performance in the simulation. In the best configuration, it is possible to see that by storing water at 90 °C (obtaining 138.78 kJ/kg from an exchange with a typical system at ambient temperature in the months of January–February) compared to the case where the water is stored at the temperature of the underground, that is 25 °C (obtaining 77.08 kJ/kg), it is possible to store 1.8 times more energy per kg of store water without affecting the surrounding medium. Finally, the efficiency of the storage system is calculated from the thermal energy that can be potentially recovered according to the input energy needed to raise the temperature of the fluid from an ambient temperature, up to the initial storage temperature of 90 °C. Due to the thermal properties of clay in the subsoil, previous efficiencies ($\eta = 0.46$) reported in aquifer energy thermal energy storages can be obtained with relatively small storages without continuous energy inlets as is the case of the majority of seasonal thermal energy arranges, with a potential to recover 70% of the inlet thermal energy under optimum conditions of the storage cavity.

1. Introduction

The global pursuit of sustainable energy solutions has reached unprecedented levels as societies grapple with the urgent need to reduce carbon emissions and mitigate climate change. The integration of renewable energy sources into the power grid has made substantial progress, yet the intermittent and unpredictable nature of renewable resources presents challenges for a reliable energy supply. As a result, the development of efficient and scalable energy storage systems has become paramount. In this context, Thermal Energy Storage (TES) in geological materials has emerged as a promising avenue, offering a unique opportunity to store and utilize surplus thermal energy from renewable and waste heat sources [1,2]. This paper seeks to shed

* Corresponding author at: Department of Applied Physics, University of Salamanca, Salamanca, Spain.
E-mail address: jgonzalezayala@usal.es (J. Gonzalez-Ayala).

https://doi.org/10.1016/j.enconman.2024.118394
Received 20 November 2023; Received in revised form 2 April 2024; Accepted 3 April 2024
Available online 9 April 2024

Nomenclature

P	Pressure (Pa)
V	Volume (m^3)
T	Absolute temperature (K)
t	Time (s)
r	Radial coordinate (m)
k	Thermal conductivity (J/m s K)
ρ	Mass density (kg/m^3)
c	Specific heat capacity (J/kg K)

Subscript

P	Constant pressure
V	Constant volume
f	Fluid
p	Pipe
s	Sand
c	Clay

Acronyms

TES	Thermal energy storage
TDEM	Time-domain electromagnetic method
TX	Transmitting loop
RX	Receiver loop
FEM	Finite elements method
ASA	Acrylonitrile-Styrene-Acrylate
PVDF	Polyvinylidene Difluoride
PFA	Perfluoroalkoxy (vinyl ether)
PPRC	Polypropylene Random Cpolymer
CLPE	Cross - linked Polyethylene

light on the potential of geological materials as reservoirs for thermal energy storage. Geological structures, such as rock formations, deep aquifers, and underground caverns, possess intrinsic properties that make them conducive to storing and retrieving vast quantities of thermal energy [3,4]. By capitalizing on the large-scale storage capacity and remarkable thermal properties of these materials, TES systems can effectively bridge the gap between energy production and consumption, ensuring a stable and sustainable energy supply [2,5]. In [6] a techno-economic model has been developed to evaluate GeoTES systems. In particular, in this case, GeoTES can be charged with two different energy sources: (1) concentrating solar thermal and (2) renewable electricity using heat pumps (henceforth known as a "Carnot Battery"). The analysis shows that this system could be used to deliver industrial process heat, in which case the LCOH is competitive (0.03 $/kWh$_{th}$) with current natural gas prices in California, however, their analysis does not dig into too much geological details.

Energy storage can be classified into short-term storage. According to some studies, the pattern of seasonal storage could satisfy 50%–70% of the annual heat demand, whereas the diurnal pattern could only meet 10%–20%. However, big challenges should be overcome, such as the large storage volumes, with greater risks of heat loss, the materials involved also should be reliable, ecological, and economical [7]. Applications include district heating [8], in greenhouses for space heating [9–13]. Seasonal underground storage systems are by no means a new subject. Some previous studies incorporating numerical simulations include the works of Nordel and Hellström [14], demonstrating a reliable large-scale solar heating system with seasonal storage. The study found a suitable system design with low energy cost at a solar fraction of about 60% or above and compared the economics of the proposed solar heating system with other, more conventional, heating systems. Several demonstration plants involving large-scale solar-heated seasonal heat storage units were constructed in Sweden during the early 1980s. The basic storage types investigated were; a water tank on the ground (Ingelstad), a concrete pit (Lambohov), vertical pipes in clay (Kungsbacka, Kullavik), and a rock cavern (Lyckebo).

In a wide classification, three technologies have potential applications in incorporating solar energy in seasonal heat storage: latent heat storage, chemical storage, and sensible heat storage. Sensible heat storage is a simple, low-cost, and relatively mature technology and has been widely implemented, with water (for example see water tank storage in [15]), rock materials, and ground and soil as the storage materials. Latent heat storage consists of isothermal phase changing storage materials that provide higher energy density than sensible storage, and chemical heat storage which are more compact and have a larger energy storage density than sensible storage and are classified as sorption and chemical reaction storage [9,16–19].

1.1. Sensible heat storage

This paper is focused on the application of sensible heat storage underground. The utilization of geological materials for thermal energy storage offers several advantages over conventional storage technologies. First and foremost, geological formations provide immense storage capacity, enabling the accumulation of thermal energy over extended periods. This feature is particularly crucial for addressing the temporal mismatch between energy production and demand, allowing excess thermal energy to be captured and stored for use during peak load periods or seasonal variations. Furthermore, certain geological materials exhibit convenient thermal conductivity, facilitating efficient heat transfer and minimizing energy losses during the storage and retrieval processes [20–22].

Underground thermal energy storage includes water tank systems, aquifer storage, and underground soil storage, mainly focused on borehole arrays, whose application is more extended compared with the case of cavern storage.

A difference between common water tank systems, which make use of containing structures made of steel or concrete, buried underground (water pits) using a stable thermal stratification status to maintain cold and hot water separated inside the tank. The two key optimization points are the conditions of stratification, where 15–20 K can be obtained with an inlet/outlet temperature difference of 70 K; and the thermal isolation of the tank, where glass wool and polyurethane are widely used.

Regarding thermal energy storage in aquifers (ATES), in [23] an overview of the development of underground gas storage in depleted natural gas reservoirs and thermal energy storage in shallow aquifers in China is revised, showing that this technology is cost-effective, including in the revision the construction status, policy environment, technical challenges, and possible new solutions. In-depth theoretical research, novel methodology, comprehensive studies on site characterization and selection, sealing performance evolution, monitoring, etc., using integrated experiments, physical simulation experiments, and numerical simulations show economic and thermal adequacy. A configuration, in particular, can be found in [24], where the performance of the storage through hydro-mechanical modeling in function on the aquifer properties is analyzed. The model of ATES makes use of at least two thermal wells, ground water is heated by solar energy, for example, and then injected into the warm well, which is recovered in the discharge phase. In Neubrandenburg since 2005 [25] an ATES of this kind has 1200 m depth and was charged with 14,300 MWh in 2005/06 and 12,800 MWh in 2007/08, and 6500 or 5900 MWh were discharged with a recovery coefficient of 46%, respectively, operating at temperatures of 80 °C. This performance, although differs from our model, will be used to compare different technologies.

In the case of boreholes vertical or horizontal tubes are inserted, the so-called borehole thermal energy storage (BTES) and duct heat

storage, respectively [8]. These tubes serve as heat exchangers, the soil is the storage medium and water is the transfer fluid. The high heat capacity and their capability to retain water, water-saturated clay, and clay stones offer good qualities for implementing BTES, which require 3–5 times more storage volume than water storage, thus, an auxiliary water buffer is necessary for large-scale systems. The thermal contact tends to be improved and the grouting materials are extensively studied [26,27].

A plant that could seasonally store industrial waste heat was designed [28] in Germany. 15,000 m^3 of soil embedded with 140 30-m-deep vertical heat exchangers were designed to store heat to meet a heating demand of 170 kW of thermal energy, saving annually 266 MWh. In [29] through six monitoring boreholes, predicted the long-term feasibility of 65-percent recovery of heat stored underground in the BTES.

Experience with high-temperature underground thermal energy storage was also obtained from the bedrock heat store in Luleå and the rock cavern in Avesta. In [14], the Authors used simulation models with TRNSYS and MINSUN and the ground storage module Daylight Saving Time and evaluated the performance of a solar-heated low-temperature space heating system with seasonal storage in the ground. They implied an economically feasible design for a total annual heat demand of 2500 MWh. Ucar and Inalli [30] presented a thermo-economic analysis of a heating system with an underground seasonal storage system using solar thermal energy using finite element methods and monthly average solar radiance data. Two storage tank geometries were compared: trapeze type and cylindrical storage. In that model, the water was heated with solar energy from an initial temperature of 10 °C. The solar fraction, depending on the solar collector area, varies with respect to the storage volume, thus, by scaling the tank size one can obtain a desired solar fraction. It is found that for the analyzed configuration, with different configurations of materials surrounding the tanks, the most active parameters are the collector area, the heat load, and the climate. And concluded that the effects of ground type on the long-term performance of the storage system are negligible, one characteristic that does not occur in a model like the one presented in this paper, as will be discussed later. In 2006, Wong, Snijders, and McClung [31] proposed a system of low/high-temperature wells for cooling and heating of spaces. The warm water is pumped out in winter and stored as a low-temperature reservoir for summer, which is later pumped out for cooling in summer and later it is heated with ambient temperature and stored for winter. Cold water is stored at 6 °C and hot water at 14 °C–17 °C. In 2009, Karacavus and Can [32] presented an economical assessment of the solar heating system with seasonal storage performed and contrasted with experimental values, and special attention was placed on the optimum collector area for the heating system. Sweet and McLeskey in 2012 [33] made the numerical simulation of a system for capturing and storing solar energy during the summer for use during the following winter. The model used a bed filled with sand as a storage system (due to its high thermal capacitance) for heating of individual residential homes via radiant homes. The upper part of the storage was located 1 m below the ground surface. Hamm and Bazargan Sabet [34] in 2010 assessed the geothermal potential of a flooded coal mine in Lorraine, France, they investigated the water temperature inside a vertical shaft and reported that this could evolve differently due to convection produced by buoyancy forces, which significantly modify the temperature at the production zone. Madiseh et al. in 2013 [35] analyzed the performance of borehole heat exchangers using natural convection with a tube length of 100 m in a closed-loop. Ghoreishi et al. in 2015 [36] performed a heat transfer analysis of large-scale seasonal thermal energy storage for underground mine ventilation utilizing naturally available renewable energy sources from seasonal cycles for heating and cooling of underground mines where heat can be stored in the broken rock as sensible heat. Zhou et al. in 2021 [37] reviewed the state-of-art of Underground seasonal thermal energy storage worldwide. Pointing out that this kind of system can overcome the instability and low efficiency of the short-term thermal storage system. However large heat loss and low solar fraction are still common challenges for large-scale applications as well as the selection of materials for long-term energy storage. It is stated also that reported data [38] shows that the solar energy seasonal heating system with underground soil as a thermal storage body can compete with the electric heating system and the conventional fuel heating system, and its annual cost is only 1/3 of the electric heating system and 2/3 of the conventional solar energy heating system. In 2023 Yang et al. [39] presented a 3-D CFD model of borehole energy storage to find the influences of borehole layout forms, layout spacing, and depths on the characteristics of these systems.

As can be seen, and as it is highlighted in [37], the fundamental research is still in an early stage, and the corresponding theoretical exploration and research are lagging behind, with current research focused mainly on underground heat exchangers, temperature field distribution, thermal and moisture transfer, with only demonstration projects of very small scale.

Regarding the modeling, some interesting approaches for optimization of multi-energy systems seizing geothermal energy storage and accounting for seasonal variability of heating and cooling demands make use of approximate behaviors of boreholes, modeled as infinite line heat sources [40] interacting with a static soil temperature field. Analytical models improve previous approaches carried out using numerical solutions given in the form of tabulated or graphic values [41] and are suitable for optimization analysis. Nevertheless, it should be noted that the general axisymmetric problem does not have an analytical solution, and more accurate behavior of the interaction between heat extraction systems and the underground requires the use of numerical simulations. In particular, in [42] this numerical approach was carried out for a set of U-shape borehole heat exchangers, where the influence of the pumping system over the surroundings is noticeable for long operation periods. Further simplification approaches have been proposed to reduce computational time [43], but exhibiting as well the limited but not negligible effect of the storage systems in the soil temperature. This has been studied in an efficient manner in [44] where the impact of borehole heat exchangers in the surrounding subsoil, considering far boundary condition of constant temperature. These approaches mainly focus on pipe configuration and heat exchanging systems in depts within 100 m.

This work aims to complementary explore the potential and advantages of utilizing subsoil clay layers as a thermal energy storage medium in depths within 500 m, although this analysis can be extended as long as an accurate thermal map of the subsoil can be deduced. Clay possesses several key characteristics that make it well-suited for TES applications. Firstly, clay exhibits convenient thermal conductivity, allowing for efficient heat transfer and minimizing energy losses during the storage and extraction processes [45]. Additionally, its high volumetric heat capacity enables the storage of substantial amounts of thermal energy within a relatively small volume, making it a space-efficient solution (see Fig. 5 in Section 4.1, below). Furthermore, clay layers can be found at suitable depths which avoid the thermal influence of the surface and are operationally favorable.

The utilization of subsoil clay layers for TES may offer several benefits and applications [46,47]. In the context of renewable energy sources, excess thermal energy generated by solar or geothermal systems can be stored within the clay layers during periods of low demand and later extracted when needed, aligning energy supply with varying demand patterns. Moreover, the integration of TES in clay layers can enhance the performance of district heating and cooling systems by smoothing out peak loads and optimizing energy utilization [48]. Additionally, the versatility of clay allows for the potential integration of other energy systems, such as ground source heat pumps, to further enhance the overall energy efficiency of buildings and infrastructure.

To comprehensively explore the potential of TES in subsoil clay layers, this paper will delve into various aspects of the subject. It will

be focused on a sedimentary formation geometrically characterized by geophysical methods, where heat exchange simulations have been carried out. Within this sedimentary formation, there is a clay layer that has sufficient thickness and extension to offer seasonal storage possibilities without thermal affectation to the upper and lower aquifers present in the sand layers that surround it. The design considerations for clay-based TES systems, such as the depth and thickness of clay layers, will also be discussed. Furthermore, case studies and experimental findings will be examined to provide insights into successful applications, system performance, and potential challenges [49].

In addition to technical considerations, this analysis can be easily complemented with environmental and economic aspects of thermal energy storage in subsoil clay layers. By reducing the reliance on conventional energy storage methods, such as pumped hydro or battery systems, clay-based TES can contribute to the reduction of greenhouse gas emissions and promote a more sustainable energy landscape. The economic viability and cost-effectiveness of TES solutions is becoming more and more convenient, considering factors such as installation costs, operational efficiency, and long-term maintenance [50]. It should be clarified that the present paper focuses on studying the system's capacity to retain energy for long periods, not relying on further energy input on the system and showing the potential for energy extraction (in terms of energy per kg of stored water) making easier to couple this analysis with any input/recovery technology. Additionally, the energy landscape for energy extraction can be useful in the analysis of multiobjective and multiparametric optimization, since these methods rely mostly on ultrafast sorting algorithms. Thus, it aims to stimulate further research, innovation, and deployment of TES systems utilizing geological formations. Ultimately, by harnessing the untapped frontier of thermal energy storage in geological materials, the present research can pave the way for a resilient and low-carbon energy future. In recent years, underground solar heat storage has been widely developed around the world with more and more attention to energy and environmental protection [37]. It is also expected to constitute a novelty regarding mid-to-shallow-depth thermal storage (considering those that allow the application of common drilling techniques used for groundwater collection in the indicated study area), yielding promising thermal simulations for seasonal storage despite the mentioned depth conditions [51].

The paper is structured as follows: In Section 2 an analysis of the terrain and the data acquisition of its composition and its thermal properties is presented. In Section 3 the heat transport model is shown. In Section 4 the analysis of the storage capacity according to the materials distribution, size effects, and isolating materials is addressed. Finally, some concluding remarks and possible storage strategies are discussed.

2. Analysis of the geological environment

A prospecting analysis on specific locations can be substantially improved with a rough knowledge of the characteristics of the soil composition on site and the temperature as a function of depth. In this sense, different kinds of soil and thermal gradient can be used for a variety of applications, and the capacity to transfer heat and the presence of natural structures can be more suitable for specific usages. In this research, an analysis of the subsoil composition in the Amblés Valley is used as a representative case (Fig. 1). However, this methodology can be reproduced in other regions.

2.1. Time Domain Electromagnetics (TDEM)

The Time Domain Electromagnetic Method usually known as TDEM emerged as a relevant innovation in the geophysical field at the beginning of the 1980s. This technique applies transient electromagnetic field diffusion under time-domain control [52] and is based on the injection of a constant current into a loop or transmitting coil (TX) that generates a constant primary magnetic field. A magnetic field perpendicular to the plane of the transmitter loop is generated as a consequence of injecting current. When this injection is turned off, the decay of the mentioned primary field induces electromotive forces within the surface, producing eddy currents that penetrate the ground, thus generating a secondary magnetic field in which amplitude decreases with time (transient). During the test, the voltage against time for the decay of the secondary magnetic field related to the eddy currents and created by the primary transmitter is measured by the receiver loop (RX) during the turn-off period. From the measuring of the decay at several intervals, a curve is obtained. The amplitude and shape of this curve reflects the resistivity distribution with depth, where early times (short time voltages) provide information about the resistivity of shallow layers while later times refer to deeper depths [53,54]. TDEM presents a clear advantage regarding the rest of electromagnetic and electrical methods; its reduced sensitivity to the separation between the transmitter (TX) and the receiver (RX) loop, being the only electrical technique capable of operating with a separation TX/RX lower than the depth of the explored structure. All the above enables the improvement of the method lateral resolution, requiring, however, longer distances for deeper prospecting to deal with the possible noise effects. The prospecting depth of TDEM is ultimately defined by time, given that the transmitter stops emitting at the related magnetic moment. If longer depths are required, it is necessary to perform the signal collection at later stages. Additional information about the physical fundamentals of TDEM can be found in previously published research [55,56].

2.1.1. Data acquisition

In this research, a total of 19 TDEM survey points were executed on the considered study area, as mentioned above, to reduce noise the survey points were spread over the zone as even as possible, according to the accessibility and clearing of the surroundings. Field data were acquired by the use of a TerraTEM device (Monex GeoScope Ltd.; The Basin, VIC, Australia) together with a TerraTX-50 transmitter. This last transmitter delivers an output voltage of 96 V and a transmitter current of 50 A operating with a GPS synchronization module. A coincident-loop configuration of 200 m × 200 m (or 150 × 150) was selected to obtain enough penetration and signal to achieve the granite basement. TDEM points locations were defined by the use of handheld 3 m accuracy GPS while topography heights were extracted from 5 m resolution DEM [57]. Additionally, TDEM survey points were distributed in a self-regular grid covering the planned area under study, where there was sufficient spacing for the loop laying and for avoiding the close presence of anthropogenic interferences. The following Fig. 1 shows the distribution of the TDEM survey points in the area under study.

2.1.2. Processing approach

After the field campaign, TDEM raw data were processed using TerraTEM equipment TEMPlot V 2.0.0 software (Monex GeoScope Ltd.; The Basin, VIC, Australia), that enables displaying the voltage/time curves, as well as automatic and manual filtering with the aim of removing wrong time windows and exporting the initial pre-processed data. Automatic filtering is used for removing data with an anomalous acquisition time/voltage. Meanwhile, through manual filtering, the time interval that will be considered in the inversion software is established.

As a second step, the commercial IX1D-V3 software (Interpex Limited; Golden, CO, USA) was used for modeling the TDEM data. This inversion tool is specifically designed for a 1D analysis of electromagnetic and electric data inversion and interpretation, thus providing 1D resistivity models and generating geoelectric resistivity versus depth columns for each TDEM sounding. The software allows the user to introduce a preliminary geoelectrical model with a predefined number of layers, thickness and resistivity values. In this sense, the available geological and lithological information was used for determining the number of layers and thickness in order to allow the inversion tool to

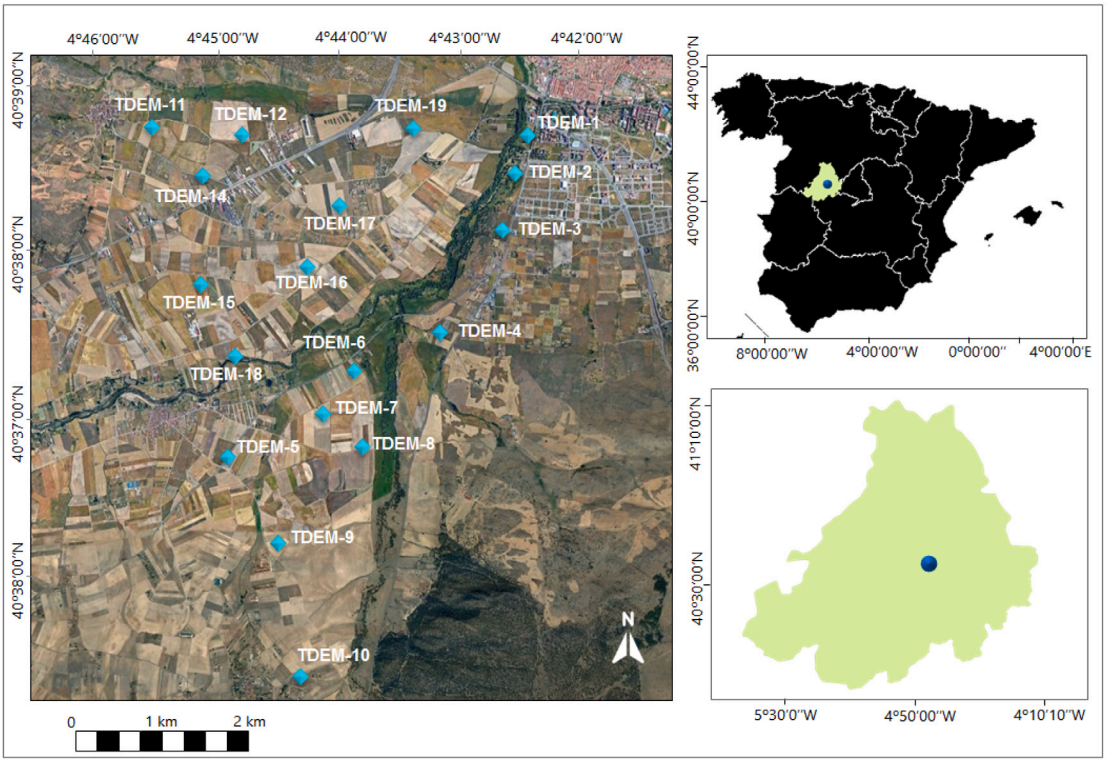

Fig. 1. Distribution of the TDEM survey points within the context of the area under study. *Coordinates are expressed in latitude and longitude.

adjust the resistivity of the layer in the model with the best fit of the model curve convergence with the survey data.

After all the steps previously described, a data joint interpolation was performed through the Oasis montaj software (Seequent) with the final objective of obtaining a 3D geoelectric model that allows an in-depth analysis of the whole subsoil distribution.

2.2. Sand and clay spatial distribution

Electric resistivity of the subsurface was inferred from the above mentioned analysis. The data contains information on a space bounded by a box of lengths 4400 m × 6700 m × 600 m in the XYZ direction. The information on the resistivity, and previous analysis of the soil in the region allows the identification of geoelectric regions, each one dominated by the presence of sand, clay, or granite. This information should be considered as an approximation, specific geological anomalies could exist, and the exact composition of the area could only be known through exploratory drilling with core extraction. In the interpretation of the obtained data, small resistivities correspond to a large presence of clays, meanwhile larger resistivities are associated with the presence of sand and gravels and, with higher resistivities, to granite. With resistivities ranging from 10 to 17.5 Ω m the composition of the soil is mainly clay and sandy clays, with isolated levels of sand, sandy clays, and gravels. This region is depicted in Fig. 2a. Clays cover a wide range of chemical compositions and their physical properties strongly depend on factors such as water saturation and porosity. Nonetheless, its low permeability and mechanical/plastic properties [58,59] make them of interest to explore natural structures where fluid can be contained for long periods. This could offer a potential use for seasonal fluid storage, in maintaining stationary flows, or in natural packed beds for thermal energy storage. In Fig. 2a it is possible to find cylindrical-shaped subregions, one of them is depicted in a close caption in Fig. 2b. A bottom view shows (see Fig. 2c) the presence of bubbles consisting mostly of clays with low resistivities. These closed sub-structures could be of potential interest due to the visible isolation of the clay.

On the other hand, the material exhibiting resistivities within the range from 17.5 to 30 Ω m is depicted in Fig. 2d, which is mostly consisting of alternating sandy clays with levels of sands, clayey sands, gravels, sandstones, and conglomerates. Higher resistivities indicate a larger concentration of sand and gravel. This region forms an upper and lower bound of the previously discussed region consisting of clays. Fig. 2e shows a close caption of a vertical cylinder crossing through the layer of clays. This region could be of interest since it could offer the combination of sandy soil contained by clays that may be of interest for packed bed applications or heat extraction, as will be discussed later.

In Fig. 3a the layer of granite is shown, with resistivities above 30 Ω m. As will be discussed below, there is a region exhibiting a steep increase in temperature. This will be used to compare the performance of energy storage before and after such a temperature gap. Since this region is always located above the granite, the granite layer is not considered for the analysis of the present study.

2.3. Temperature with depth

As it is well known, temperature in the underground increases with depth. However, its increments are by no means constant. The temperature profile with depth can vary according to many factors such as the presence of aquifers, thermal properties of the soil in the specific location and granite layers (which could transport heat from the mantle more efficiently than granular medium), among others.

In the region, temperature profiles ($T(z)$) were measured with existing piezometers at every 25 m depth until a depth of 500 m. Temperature measurements were recorded by a single-channel HOBO U12 temperature data logger (range: −40 °C to 125 °C, resolution: 0.03 °C, accuracy: ±0.25 °C). The points where the temperature was measured are depicted with dots in Fig. 3a (see the vertical dotted lines). In each temperature profile, the increments of temperature were obtained and those that exhibited unusually large gaps between measures were marked in red (see Fig. 3a). To explain the unusual increase in temperature a search for correlations between the fitted thermal conductance

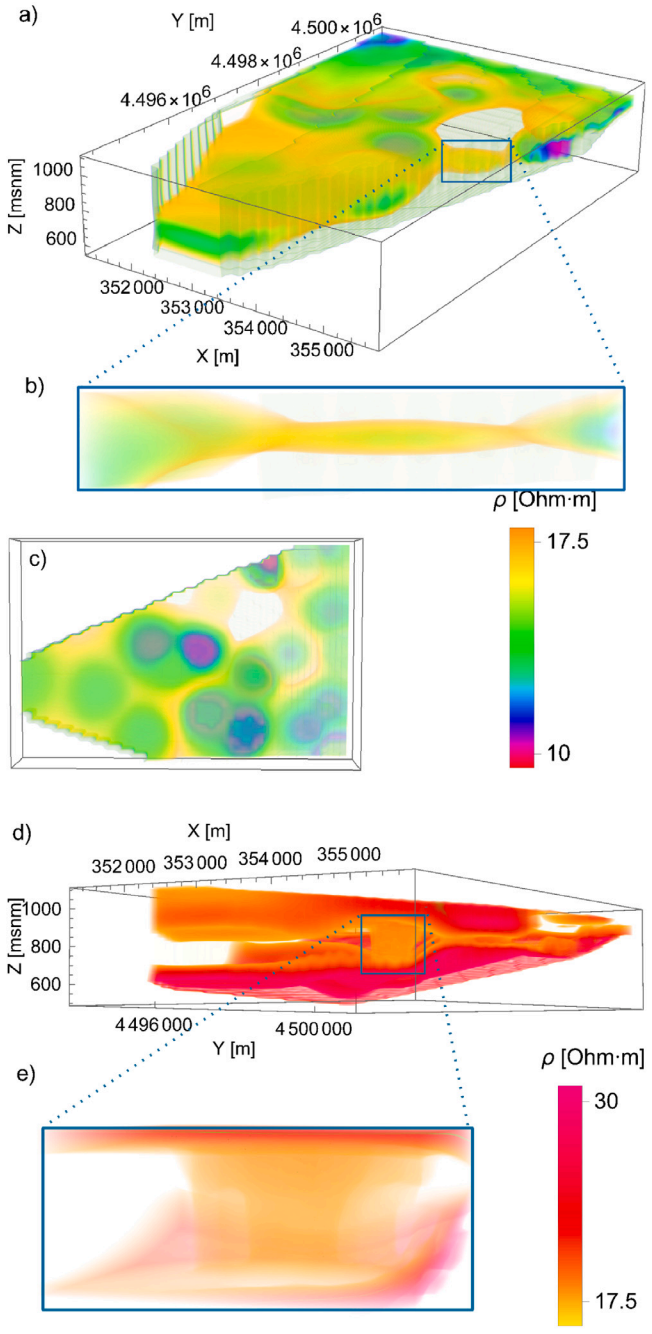

Fig. 2. (a) Representation of the electric resistivity of the soil. A TDE analysis of the soil in the region of Avila provides a rough vision of sub-structures containing mostly clays, with isolated sandy regions. The depicted sub-region is located in the Ambles Valley and it is within a volume of lengths 4400 m × 6700 m × 600 m in the XYZ directions. In (b) a close-caption of an isolated cylindrical sub-region. In (c) a bottom view of the region. the presence of spherical-shaped subregions in the deeper zones, which is consisting of the higher density of the clays with respect to sands. (d) Representation of the electric resistivity of the soil in the range from 17.5 to 30 Ω m. This region forms an envelope of the previous region consisting mostly of clays. In (e) a close caption of a subregion with cylindrical geometry crossing vertically through the clay layer.

(according to the electric resistance), was carried out. In some of these points, the heat transport obtained does not correspond to only heat conduction, following the Fourier law of heat conduction. Thus, another transport mechanism should take place (such as convection), pointing out the presence of water. However, the correlation between these two phenomena is not high enough, and further analysis of the

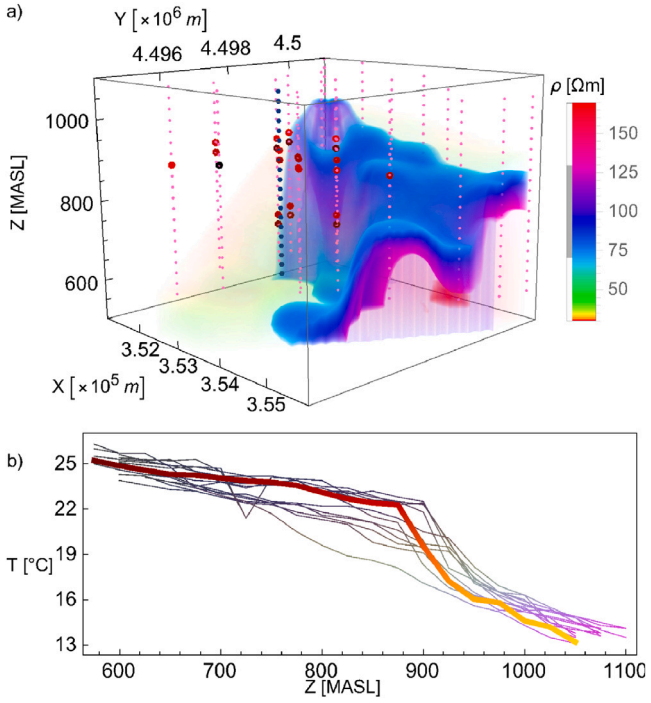

Fig. 3. In (a) The temperatures measured (small pink dots) in 19 locations (on the surface). The bottom surface indicates the granite layer. The large red points above the granite indicate large thermal gradients which can be seen in (b), where the temperature curves are depicted for each site. Notice that the rapid increases in temperature occur in the gap between 880 and 960 m above sea level (140 to 220 m depth). The highlighted curve shows the temperature measured in El Fresno, Avila (Spain) located at coordinates (40.61982535618638, −4.745582841984521).

place should be made to guarantee the cause of the increase in temperature. The temperature as a function of depth is shown in Fig. 3b. As a particular case, the temperature measured at El Fresno, (Avila, Spain) located at coordinates (40.61982535618638, −4.745582841984521) ((X_{UTM}, Y_{UTM}) = (352350, −4498020), ETRS 89 UTM Zone: 30), is marked with blue dots in Fig. 3a and with a thick line in Fig. 3b. This temperature exhibits two regions where the increase in temperature is larger. This occurs in the gap from 100 to 200 m in depth. From this 200 to 500 m the temperature increase is constant but slow. This study will focus mainly on the temperature of 298.15 K (25 °C) which roughly is the largest value measured in the region. It is expected that at this point the largest amount of energy can be extracted, or the least amount of energy is lost by the thermalization of a hot fluid.

A first approach to studying the interaction between storage fluids and their surroundings will be made through a simple model with a cylindrical geometry including different combinations of layers. Nonetheless, the presence of long cylindrical and spherical substructures might well justify the seizure of this simplification.

3. Thermodynamic model

The mathematical model consists of a series of concentric cylindrical regions. The inner part corresponds to the fluid that will be stored at a constant initial temperature $T_{f,0}$ along the length of the cylinder. The storage fluid is water. Energy flows due to the temperature gradient to the surroundings. The variables to analyze are the size of the storage region, the alternating layers of clay and sand that surround it, the depth at which it is located (affecting the pressure and the temperature of the surroundings) and the possible use of isolation layers or pipelines. This configuration is schematically depicted in Fig. 4.

The analysis of [60] in BTES suggests that heat extraction efficiency increases with decreasing soil thermal conductivity, the efficiency decreases with background groundwater flow and with convective heat

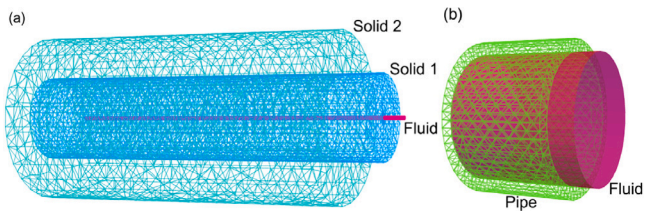

Fig. 4. In (a) the thermodynamic Universe of the system. The fluid is water, and the presence of the pipe containing the fluid is included. Solids 1 and 2 can be sand and clay, respectively, or vice versa. A comparison of both cases is presented in the following section (see Fig. 5). The thickness of each domain will be subject to optimization as will be depicted in Fig. 6 and an ideal material and thickness for solid 1 will be given (at the conclusions). In (b) a close caption of the fluid and the optional pipe element.

losses associated with high soil permeability values, and unsaturated soils show higher overall heat extraction efficiency due to convection onset at higher intrinsic permeability values.

The effect of fluid temperature on the surroundings over extended periods is the major concern of this work. Thus, it will be assumed that the period in which the fluid is charged into the system is quite short compared with the storage period, so the input and output processes are not analyzed. The mathematical model will only consider the effect of heat conduction over the different solid layers, comparing different isolating materials for the pipe. According to the literature, for energy storage in clay, the low permeability (around 10^{-9} m/s) justifies the neglection of convective heat loses [61,62] if the water flow exceeds 50 mm/day a screen is required to reduce water flow [63].

In the absence of heat sources, the transient heat equation includes only a diffusion term that accounts for the conduction of heat between the different layers of the system, then, the conductive heat equation is [64]

$$\rho c_X \frac{\partial T}{\partial t} - \nabla (k \nabla T) = 0 \tag{1}$$

where ρ is the density of the material, c_X is the specific heat capacity at constant volume (for the storage fluid) or constant pressure (for the solid exterior layers) and T is the absolute temperature of the material and t is the time variable. Due to the symmetry of the system, a cylindrical coordinate system transform Eq. (1) into

$$\rho c_P \frac{\partial T}{\partial t} - \frac{1}{r}\frac{\partial}{\partial r}\left(k\, r \frac{\partial T}{\partial r}\right) = 0 \tag{2}$$

where invariance on the angular direction and the length of the cylinder are assumed since the cylinder is long. Therefore, a 1-dimensional problem will suffice for this analysis, and the only spatial variable of interest is the radius, r. Eq. (2) is valid for the different layers. A finite-elements methods approach will be used to obtain the temperature profile $T = T(t, r)$. The mesh for the different radii is made through the cumulative function of the thicknesses $\{0, r_f, r_p, r_s, r_c\}$ which indicate the radius at which each layer ends. The differential equation is numerically solved in Wolfram Mathematica ©, defining in each domain the corresponding thermal properties. For water, they were obtained from the NIST database considering that water at high pressure and in a wide range of temperatures will experience thermal coefficients dependent on these two variables. Here it is considered an isobaric cooling process, the pressure of the water is $P_0 = 50$ bar, which is the minimum pressure that the fluid should experience to be extracted ($\rho g h \approx 49$ bar). The resulting thermal properties depend on temperature as follows,

$$\begin{aligned} \rho_{water} &= 248.373 + 6.7T - 0.01874T^2 + 1.5833 \cdot 10^{-5}T^3, \\ c_{p,water} &= 3845.83 + 5.572T - 0.0156T^2, \\ k_{water} &= -0.7265 + 0.007316T - 9.5215 \cdot 10^{-6}T^2. \end{aligned}$$

The thermal properties for the different pipe materials and measured properties of sand and clay in the region are indicated in Table 1.

Table 1
Thermal properties of the different materials included in the simulations.

	ρ (kg/m^3)	c_p (J/Kg K)	k (J/m s K)
Pipe			
ASA [65]	1100	1300	0.18
PVDF [66]	1780	1300	0.2
PFA [67]	2150	1047	0.209
PPRC [68]	895	2000	0.24
CLPE [68]	930	2300	0.41
Steel [68]	7850	440	53
Sand	1700 [69]	910 [70]	1.7 [71]
Clay	1762 [71]	1350 [71]	0.346 [71]

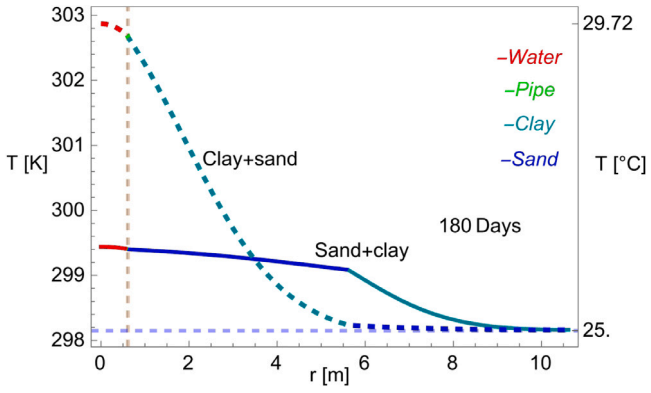

Fig. 5. Comparison of the temperature profile in the radial direction r when the domain of solid 1 and solid 2 (see Fig. 4) are either clay and sand, respectively, of sand and clay, respectively. The thermalization period is 180 days. The initial temperature is 90 °C. The surroundings of the fluid are initially at 25 °C, in equilibrium with the corresponding underground temperature (depth 500 m). The pressure of water inside the pipe is considered to be 50 bar.

The time-dependent solution to the heat equation considers an initial water temperature of $T_0 = 363.15$ K (90 °C), with an environment temperature of 298.15 K (25 °C). The radius of the total system is such that, at the farthest point, the effect of heat transport can be neglected. In the simulations this means that the difference in the temperature of the system in the boundary with respect to the environment temperature after 180 days is not larger than 5 mK. The code was implemented in Mathematica, using the finite elements method package.

4. Results and discussion

4.1. Soil distribution

The resulting radial temperature of the thermalization process over 180 days is depicted in Fig. 5. The temperature of the fluid is considerably different in a situation where the envelope of the pipe is clay or sand. The thermal properties of clay and sand are shown in Table 1, which are parameters obtained from local measures. Notice that as expected, since the clay is worst at conducting heat, it works better to store energy, leading to a sensibly higher fluid temperature after six months, in agreement with the results of [61] (see below). On the other hand, when the purpose of the system is to extract heat, sand would perform better since it thermalizes the water with the temperature of the surroundings more efficiently. Thus, for energy storage the configuration of clay+sand will be analyzed.

4.2. Size effects

An optimum design should include the prediction of efficient, or best compromise-based configuration. In this way, it is interesting to dig-in for possible improvements in the dimensions of the system,

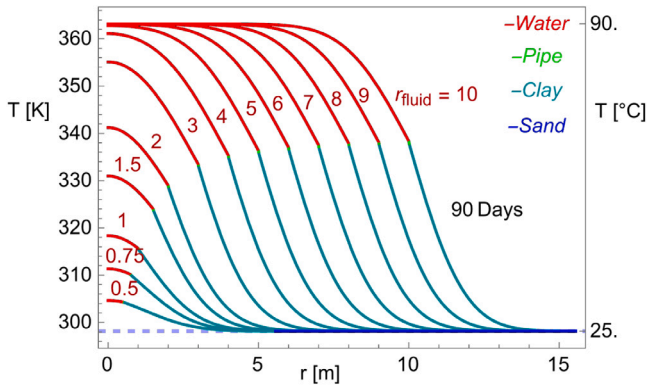

Fig. 6. Temperature profile in the radial direction r for a storage time of 90 days changing the radius of the fluid region from 0.5 m to 5 m. The initial temperature of the water is 90 °C and the solids initially are at 25 °C, in equilibrium with the corresponding underground temperature (depth 500 m). Pressure is considered to be 50 bar.

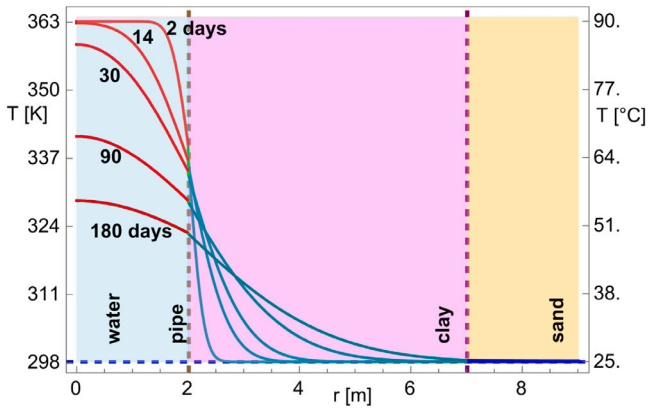

Fig. 7. The temperature profile in the radial direction r for different storage times: 2, 14,20,90 and 180 days of storage. The initial temperature of the water is 90 °C and the solids initially are at 25 °C, in equilibrium with the corresponding underground temperature (depth 500 m). Pressure is considered to be 50 bar.

potentially leading to novel/attractive solutions in underground energy storage. One variable that largely affects in the thermalization process is the mass of the storage fluid. As the mass of water increases, its temperature is expected to present smaller variations with time. A comparison between different radius for a given time is shown in Fig. 6. It can be noticed that the temperature of the fluid does not change significantly beyond a radius of 3 m. Then, larger radius will not improve the capacity to store energy. From now-on the value of 2 m will be used as an efficient configuration. Wider storing regions are expected to involve more initial costs. However, a trade-off between these two variables requires a thermoeconomical analysis, which is out of the scope of the present paper.

The comparison depicted in Fig. 7 shows the temperature profile for different storage periods. The temperature of the fluid remains higher than that of the surroundings. Notice that for large storage periods, the fluid has not perturbed a region beyond a few meters. The variation in temperature is noticeably smaller as time increases, as can be seen by comparing the difference between 30 to 90 days, with that from 90 to 180 days.

To compare the effect of thermalization on the surroundings it is possible to compare with reported results for numerical models assuming solely heat conduction which show that for single and double U-pipes with mean store temperatures of 60 °C the measured temperature spread in the clay after 6 months of operation was 8.2 m, meanwhile the calculated one was 10.5 m in a configuration of a cylinder of 5 m of radius, at 6 m depth. Given the same conditions of the soil temperature, in our model the radius of thermal influence (according to the definition of [61], where the change of temperature decreases below 0.5 °C) gave a radius of 8.22 m when the initial temperature was 90 °C, leading to a final temperature of 77 °C. If the initial temperature is 70 °C, then the final temperature is 60 °C and the influence radius is 7.95 m, also in agreement with the measured one of 8.2 m.

4.3. Insulation materials

Another feature of interest is the possible requirements of an insulating layer. Insulation thermoplastic pipes are becoming a great solution in piping and plumbing. With a growing application in oil and gas extraction because they do not corrode and have low maintenance costs. Recently, thermoplastic alternatives for storing and transporting gases and fluids have gained attention for their durability and better-isolating properties. New materials are under study. Plastic materials are more easily produced, stored, and transported, making them an attractive solution, especially for non-common applications. In the present case,

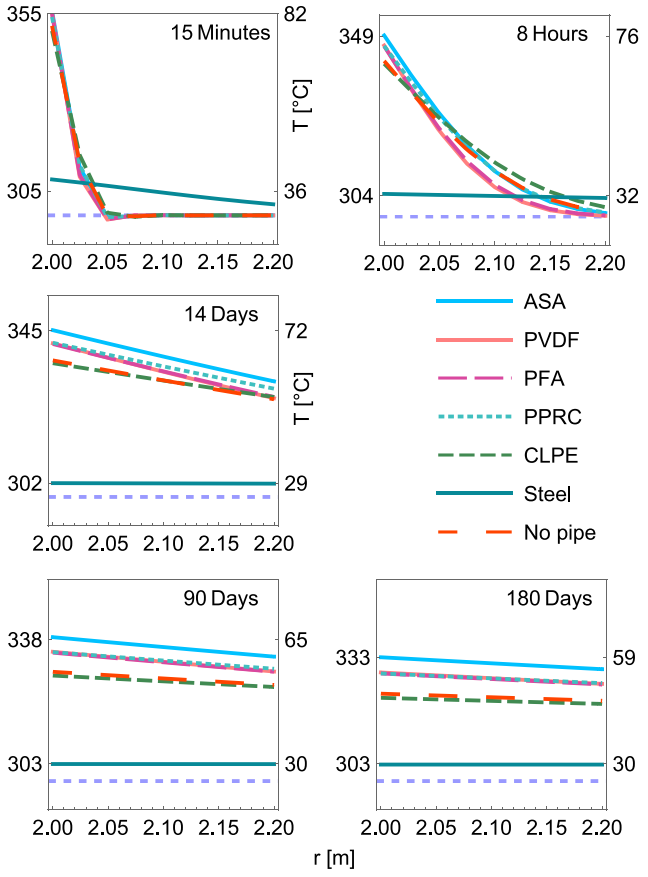

Fig. 8. The temperature profile of the pipes' radial section. The thickness of the pipeline is considered from 0 to 10 cm. Depending on the thickness of the pipe the first layer of the clay will start with a different temperature. The radius of the fluid has been set to 2 m since for a larger radius the temperature of the fluid stops changing noticeably (see Fig. 6). The case where there is no pipe is considered to compare the effect of the containing layer, in such case, the fluid is in direct contact with the clay.

as seen in Fig. 6, nonstandard containing thickness might offer a better solution for improving storage efficiency. For this analysis, some commercial thermoplastic materials are analyzed in the simulation. For comparison purposes, the cases where there is no pipe as well as the case of a steel pipe are included. The corresponding thermal properties of these materials are found in Table 1. The radius for the fluid is set to

2 m. The pipe temperature profile of several thicknesses and materials are shown in Fig. 8, where the thickness of the pipe ranges from 5 mm to 20 cm. Thus, the clay region can start at any point, from 0.5 mm to 20 cm.

After 15 min, the thermalization of the pipe is such that, except in the case of steel, the temperature changes are sensible until a radius of 5 cm. Thus, the exterior is not perturbed by the thermalization process beyond this radius. After 8 h, in the case of steel pipe, water is in equilibrium with the clay. Meanwhile, in the rest of the pipes, the water remains at a considerably higher temperature and the clay has increased its temperature by a small amount at a thickness of 20 cm. After 30 days the thickness is less relevant in keeping the water at a high temperature and the difference among pipes is noticeable. Remarkably, clay performs better than CLPE in the long run. PVDF, PFA, and PPRC have practically the same performance. The ASA case exhibited the best thermal performance, although it is clear that other considerations should be made in multiobjective thermo-economic optimization, such as costs, maintenance, or resistance to high pressures.

4.4. Maximum energy recovery

The maximum amount of energy that can be recovered by kg of stored water will be calculated. First, Fig. 9a shows the mean temperature of the water, given by [72]

$$\langle T_f \rangle = \frac{1}{r_{fluid}} \int_{r=0}^{r_{fluid}} T(r,t)dr \tag{3}$$

for a variety of radius and storage periods. Short dashed lines indicate temperatures of 40, 60, and 80 °C, medium-sized dashed curves indicate storage periods of 50, 100, and 150 days, meanwhile continuous lines indicate radii of 2 m and 3 m. Notice that the variation between these two lines is small.

It is also of interest to analyze the difference in energy recovered when comparing the case where the water is stored at a high temperature, compared with the case where the water is not heated. The change in internal energy per mass unit between these two scenarios, $\delta\bar{U}$, is given by

$$\begin{aligned}\delta\bar{U} &= \frac{\delta U}{m} = \frac{1}{m}\left(\langle U\rangle - U|_{T_{500}}\right)\\ &= \frac{1}{m}\int_{r=0}^{r_{fluid}} \frac{C_V(T(r,t))T(r,t)}{V} 2\pi L r dr - c_v T\ |_{T_{500}}\\ &= \frac{2}{r_{fluid}^2}\int_{r=0}^{r_{fluid}} c_V(T(r,t))T(r,t) r dr - c_v T\ |_{T_{500}}\end{aligned} \tag{4}$$

where T_{500} is the water in equilibrium with the underground temperature at 500 m of depth. The cost of heating the fluid can provide an estimate of the possible profit of directing the renewable energy into the storage system.

Finally, after the storage time, the recovered water is put in contact with a heat exchanger and the water reaches equilibrium with the ambient temperature at the surface, T_{Avila}, which is calculated as the average temperature in Avila, Spain, in January and February for the years 2005–2020, being $T_{Avila} = 2.606$ °C [73]. The maximum amount of energy that can be extracted from the reservoir is given by the difference in internal energy between the two states, ΔU,

$$-\Delta U = \frac{2}{r_{fluid}^2}\int_{r=0}^{r_{fluid}} c_V(T(r,t))T(r,t) r dr - c_v T\ |_{T_{Avila}} - g\cdot h, \tag{5}$$

where $g \cdot h$ is the work per mass unit necessary to bring the storage fluid to the surface. Both δU and ΔU are depicted in Fig. 9b.

5. Concluding remarks

Insights on the optimum use and design of underground TES have been analyzed. The effect of the size of the storage and depth are

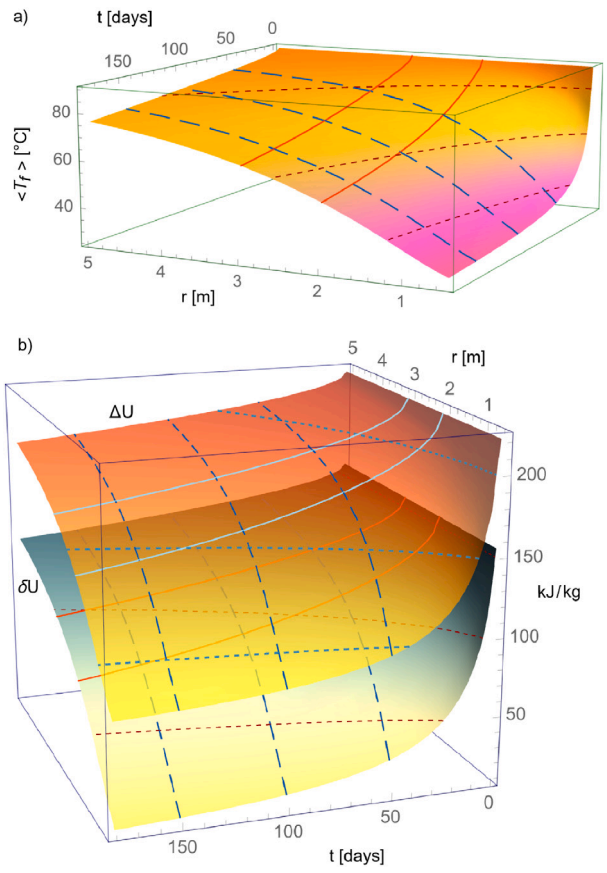

Fig. 9. In (a) the mean temperature of the water for the range of radii $\in (.5, 5)$ m and from 0 to 180 days. In (b) the potential energy gain, δU, compared with the scenario where the water is stored at the underground temperature (no previous heating), that is, the excess of energy obtained by heating the water before the storage period, and the maximum energy that can be extracted from every kg of water at the end of the storage period, ΔU. Short dashed lines are placed to indicate mean temperatures of the fluid of 40, 60, and 80 °C medium-sized dashed curves indicate storage periods of 50, 100, and 150 days, and continuous lines indicate the radius of 2 m and 3 m, which appear as optimum values.

factors that can influence in a relevant way the energetic cost of heat extraction.

As can be seen in Fig. 3b the temperature map on the region exhibits a monotonous increase of the temperature with depth, however, this growth is not uniform. So far, a depth of 500 m has been used since it represents the higher value of the environment temperature. Nevertheless, large depths can represent a drawback in the implementation of these kinds of TES systems. Fig. 3b shows a big increase in temperature between 200 and 300 m depth. To compare the benefits of putting into place a TES at higher temperatures, that is, at higher depths, the mean temperature of the fluid and maximum energy extractable is obtained. Three cases are under study: the ASA case, which exhibited the best (B) performance. This case is compared with the case of a standard steel pipe, which corresponds to the worst performance (W), with a nominal diameter of 1200 mm with a dimension schedule SCH 80, which has a thickness of 1.27 cm. And the third case is the one with no pipe material. The underground temperatures and pressures used are presented in Table 2 along with the radius of the inner cylinder where the fluid is stored and the corresponding thickness of the container walls.

The thermal properties of water at the given temperature and pressure are from the NIST database, and the comparison stemming from the simulation appears in Fig. 10. The mean temperatures for a given time are shown in Fig. 10a. Meanwhile, the maximum recoverable

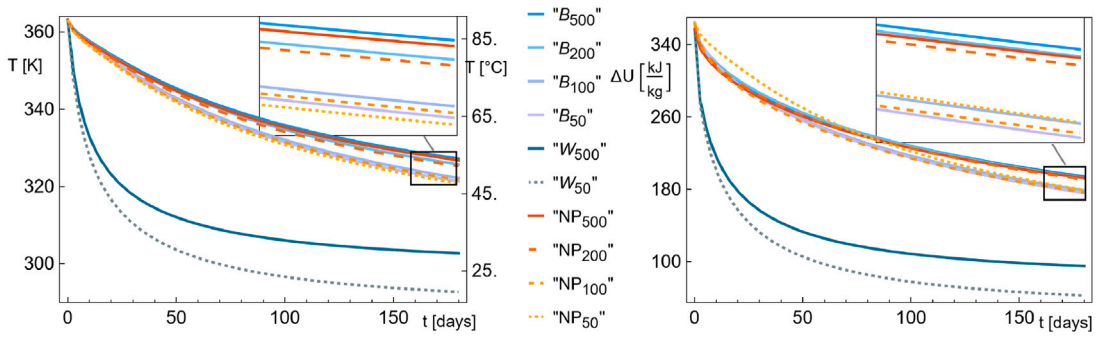

Fig. 10. In (a) the fluid temperature for the best (B) and the worst (W) pipe configurations. In (b) The corresponding maximum recoverable energy. The case with no pipe is also depicted for comparison purposes.

Table 2
Parameters used for the comparison of the best and the worst configurations.

Depth [m]	50	100	200
Temperature [°C]	14.2	15.81	22.28
Pressure [bar]	6	11	21
Pipe	ASA (Best)	Steel (Worst)	No pipe
Fluid radius [m]	2	0.6	2
Thickness [m]	0.05	0.0127	–

Table 3
Realized seasonal sensible heat storage projects [7]. DE = Germany, SE = Sweden, IT = Italy.

Project	Demand by district heating (GJ/a)	Storage volume (m^3)	$\frac{\text{Energy}}{\text{volume}}$ (GJ/m^3)
Calabria, IT (Pit) [74]	111	500	0.22
Rostock, DE (Aquifer) [75]	1789	20,000	0.09
Stuttgart, DE (Gravel) [76]	360	1050	0.34
Neckarsulm, DE (Duct) [75]	5987	20,000	0.3
Attenkirchen, DE (Duct) [77]	1386	500 (hot water) +10,500 (duct)	0.13
Anneberg, SE (Duct) [78]	1980	60,000	0.03
Lidköping, SE (Duct) [79]	3528	15,000	0.24

energy is in Fig. 10b. For the steel pipe, it is noticeable that the temperature gap between a storage chamber at 50 m and 500 m is the largest of all. For the rest of the cases, the difference is small. There is a sensible increase in temperature and energy in the region from 100 to 200 depth, where there is a pronounced increase in temperature. The gain from 200 to 500 m of depth might not justify the initial investment. An interesting feature is the convenience of having the storage chamber near the surface. Notice that for storage periods of 2 months, the best energetic outcome is in the case where there is no pipe (water is just surrounded by clay). Additionally, in this configuration, the case at 50 m is always better than at 100 m since the energy required to extract the water is not compensated by the increase in temperature due to the depth.

In the best configuration, with the ASA material as the thermoplastic cover, a 2 m diameter cylindrical deposit at 50 m depth, and in an exchange with a typical system at ambient temperature in the months of January-February, the maximum extractable energy per kg of water is 138.78 kJ/kg with water at an initial temperature of 90 °C, this can be compared to the case where the water is stored at the temperature of the underground, that is 25 °C, in which case it can be recovered 77.08 kJ/kg. Thus, with an inlet at a hot temperature, it is possible to store up to 1.8 times more energy per kg of stored water than without previous heating and, as can be seen in Figs. 6 and 7 with a limited impact on the surroundings of the storage system. Since the goal is to store excedent energy from renewable sources, such as solar energy, and since these results can scale, a location with a storage volume of 1000 m^3 can store around 200 MW, for example. This can be attractive for different energetic strategies, including the possibility of having distributed TES for local supply.

As can be seen from Fig. 9b, by comparing the design of [28], the annual saving of energy of 266 MWh could be obtained (optimistically) from our system in a configuration with radius of 5 m ($\Delta U \approx 180$ kJ/kg ≈ 180 MJ/m^3) and a length of 68 m, or with a length of 85 m if a heat leak of 20% is considered. In [7] a list of realized seasonal sensible heat storage projects are compared. In Table 3 a list of the projects that are similar in capacity to our system in terms of energy demand per storage volume is presented. The reference of this paper is that the best configuration offers annually 0.18 GJ/m^3.

The range of final temperatures depicted in Fig. 9a are just above the reported temperatures in thermal energy storage in unsaturated

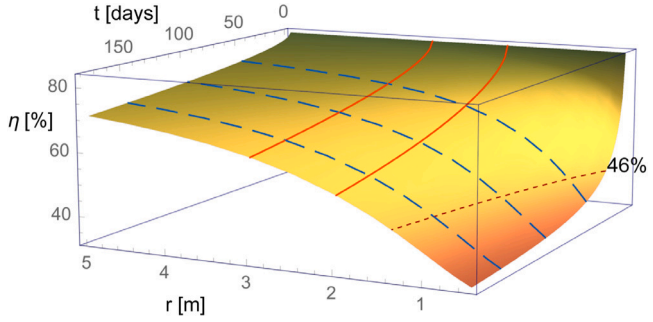

Fig. 11. Efficiency of the thermal energy storage system as a function of storage time, t and radius of the storage, r.

soils [80], where evolution in temperature and degree of saturation in soil layers having different hydraulic properties and water table depths were simulated during five years of operating a group of five energy piles with inlet fluid temperatures of 90 °C during heat injection and 30 °C during heat extraction. Transient fluctuations in the degree of saturation were observed in all soil layers simulated, but a permanent decrease was only observed for a soil layer having a greater air entry suction after several cycles of heating and cooling. This influence of air entry was not evaluated in our analysis due to the analyzed depths. This could explain the larger temperatures obtained. Model tests reported in [49] to investigate the potential effect of the heat and moisture coupling migration on the heat transfer characteristics of buried pipes show that the thermal conductivity of lateritic clay increases with increasing soil temperature due to the latent heat transfer of vapor. For lateritic clay with an initial saturation of 13.42%, the thermal conductivity increases to 7.3 times that of 5 °C at 90 °C. Simulation results show that the influence of the initial soil moisture on the heat and moisture coupling migration should be taken into account when accurately evaluating the performance of the Soil Thermal Storage system.

In Fig. 11 it is possible to see the efficiency of the thermal energy storage system, this efficiency is given by the ratio

$$\eta \equiv \frac{E_{outlet}}{E_{inlet}}, \tag{6}$$

where E_{inlet} is the energy necessary to increase the temperature of water in the summer, from around 20 °C to 90 °C, meanwhile E_{outlet} is the energy obtained in a discharge process cooling down the water to a final temperature of 5 °C. Efficiencies of 46% as those reported in [25] in ATES systems can be achieved with a relatively small radius, as can be seen in Fig. 11. The obtained efficiencies are also within the range of reported efficiencies of 65% [29].

This analysis does not assume the origin of the energy source in the charging stage and makes no reference to the discharge technology, giving a wide spectrum for using the stored energy. The results stemming from this analysis can be implemented directly in a coupling with specific technologies. Additionally, the potential for energy extraction presented in surface obtained in Fig. 9 can be used in further multi-objective and multiparametric optimization strategies, which usually make use of fast sorting algorithms, and are difficult to integrate with time-dependent dynamic systems.

Further analysis including energetic demand, economic costs for implementation, and maintenance can be included in a further thermoeconomical analysis for a complete evaluation. Nevertheless, this first approach already points out an existing energetic trade-off for an initial setup that could be of interest.

CRediT authorship contribution statement

J. Gonzalez-Ayala: Writing – original draft, Visualization, Software, Methodology, Investigation, Formal analysis. **C. Sáez Blázquez:** Writing – review & editing, Methodology, Investigation, Data curation. **S. Lagüela:** Writing – review & editing, Supervision, Project administration, Investigation, Funding acquisition, Conceptualization. **I. Martín Nieto:** Writing – review & editing, Supervision, Project administration, Investigation, Funding acquisition, Data curation, Conceptualization.

Declaration of competing interest

The authors declare that they have no known competing financial interests or personal relationships that could have appeared to influence the work reported in this paper.

Data availability

Data will be made available on request.

Acknowledgments

This project has been supported by NEXTGENERATION EU funds under project MIA.2021.M01.0004.E24. The authors also thank the Ministry of Science and Innovation, Government of Spain, for the financial support given through the project 2022/00397/001. In addition, CSB acknowledges the grant RYC2021-034720-I funded by the Ministry of Science and Innovation MCIN/AEI/10.13039/501100011033 and by the European Union "NextGenerationEU"/PRTR.

References

[1] Sadeghi G. Energy storage on demand: Thermal energy storage development, materials, design, and integration challenges. Energy Storage Mater 2022.
[2] Mahon H, O'Connor D, Friedrich D, Hughes B. A review of thermal energy storage technologies for seasonal loops. Energy 2022;239:122207.
[3] Kallesøe AJ, Vangkilde-Pedersen T, Guglielmetti L. HEATSTORE–underground thermal energy storage (UTES)-state of the art, example cases and lessons learned. In: Proceedings world geothermal congress. 2020, p. 1.
[4] Arvanitis A, Koutsovitis P, Koukouzas N, Tyrologou P, Karapanos D, Karkalis C, Pomonis P. Potential sites for underground energy and CO2 storage in Greece: A geological and petrological approach. Energies 2020;13(11):2707.
[5] Li Z, Lu Y, Huang R, Chang J, Yu X, Jiang R, Yu X, Roskilly AP. Applications and technological challenges for heat recovery, storage and utilisation with latent thermal energy storage. Appl Energy 2021;283:116277.
[6] McTigue JD, Zhu G, Akindipe D, Wendt D. Geological thermal energy storage using solar thermal and carnot batteries: techno-economic analysis. (No. NREL/CP-5700-87000), Golden, CO (United States): National Renewable Energy Laboratory (NREL); 2023.
[7] Xu J, Wang RZ, Li Y. A review of available technologies for seasonal thermal energy storage. Sol Energy 2014;103:610–38. http://dx.doi.org/10.1016/j.solener.2013.06.006.
[8] Schmidt T, Mangold D, Muüller-Steinhagen H. Seasonal thermal energy storage in Germany. In: ISES solar world congress, 14.-19. June. Göteborg, Schweden; 2003.
[9] Alkilani MM, Sopian K, Alghoul MA, Sohif M, Ruslan MH. Review of solar air collectors with thermal storage units. Renew Sustain Energy Rev 2011;15:1476–90.
[10] Sethi VP, Sharma SK. Survey and evaluation of heating technologies for worldwide agricultural greenhouse applications. Sol Energy 2008;82:832–59.
[11] Bricault M. Use of heat surplus from a greenhouse for soil heating. In: Proceedings of the international conference on energex. Vol. 82, Regina; 1982, p. 564–8.
[12] Kavin J, Kurtan S. Utilization of solar energy in greenhouse, greenhouse heating with solar energy. REU technical series 1, ENEA, Roma: FAO; 1987, p. 178–85.
[13] Santamouris M, Balaras CA, Dascalaki E, Vallindras M. Passive solar agricultural greenhouses: a worldwide classification and evaluation of technologies and systems used for heating purposes. Sol Energy 1994;53:411–26.
[14] Nordell B, Hellström G. High temperature solar heated seasonal storage system for low temperature heating of buildings. Sol Energy 2000;69:511–23.
[15] Novo AV, Bayon JR, Castro-Fresno D, Rodriguez-Hernandez J. Review of seasonal heat storage in large basins: water tanks and gravel-water pits. Appl Energy 2010;87:390–7.
[16] Farid MM, Khudhair AM, Razack SAK, Al-Hallaj S. A review on phase change energy storage: materials and applications. Energy Convers Manage 2004;45:1597–615.
[17] Hasnain SM. Review on sustainable thermal energy storage technologies, part I: heat storage materials and techniques. Energy Convers Manage 1998;39:1127–38.
[18] Jegadheeswaran S, Pohekar SD, Kousksou T. Exergy based performance evaluation of latent heat thermal storage system: a review. Renew Sustain Energy Rev 2010;14:2580–95.
[19] Carrillo AJ, González-Aguilar J, Romero M, Coronado JM. Solar energy on demand: A review on high temperature thermochemical heat storage systems and materials. Chem Rev 2019;119:4777–816. http://dx.doi.org/10.1021/acs.chemrev.8b00315.
[20] Liu J, Wang F, Cai W, Wang Z, Li C. Numerical investigation on the effects of geological parameters and layered subsurface on the thermal performance of medium-deep borehole heat exchanger. Renew Energy 2020;149:384–99.
[21] El Alami K, Asbik M, Agalit H. Identification of natural rocks as storage materials in thermal energy storage (TES) system of concentrated solar power (CSP) plants–A review. Sol Energy Mater Sol Cells 2020;217:110599.
[22] Li B, Zhang J, Yan H, Zhou N, Li M, Liu H. Numerical investigation into the effects of geologic layering on energy performances of thermal energy storage in underground mines. Geothermics 2022;102:102403.
[23] Liu H, Yang C, Liu J, Hou Z, Xie Y, Shi X. An overview of underground energy storage in porous media and development in China. Gas Sci Eng 2023;205079.
[24] Birdsell DT, Saar MO. Modeling ground surface deformation at the swiss HEATSTORE underground thermal energy storage sites. In: World geothermal congress. WGC 2020+ 1, ETH Zurich, Institute of Geophysics; 2020, p. 22046.
[25] Kabus F, Wolfgramm M. Aquifer thermal energy storage in neubrandenburg - monitoring throughout three years of regular operation. ffstock'2009. In: 11th international conference on thermal energy storage. Stockholm, Sweden; 2009.
[26] Gustafsson AM, Westerlund L, Hellström G. CFD-modelling of natural convection in a groundwater-filled borehole heat exchanger. Appl Therm Eng 2010;30:683–91.
[27] Delaleux F, Py X, Olives R, Dominguez R. Enhancement of geothermal borehole heat exchangers performances by improvement of bentonite grouts conductivity. Appl Therm Eng 2012;33–34:92–9.
[28] Reuss M, Beck M, Müller JP. Design of a seasonal thermal energy storage in the ground. Sol Energy 1997;59:247–57.
[29] Rapantova N, Pospisil P, Koziorek J, Vojcinak P, Grycz D, Rozehnal Z. Optimisation of experimental operation of borehole thermal energy storage. Appl Energy 2016;181:464–76.
[30] Ucar A, Inalli M. Thermal and economical analysis of a central solar heating system with underground seasonal storage in Turkey. Renew Energy 2005;30:1005–19.

[31] Wong B, Snijders A, McClung L. Recent inter-seasonal underground thermal energy storage applications in Canada. In: 2006 IEEE EIC climate change conference. Ottawa, ON, Canada; 2006, p. 1–7. http://dx.doi.org/10.1109/EICCCC.2006.277232.

[32] Karacavus Berrin, Can Ahmet. Thermal and economical analysis of an underground seasonal storage heating system in thrace. Energy Build 2009;41:1–10.

[33] Sweet ML, McLeskey Jr JT. Numerical simulation of underground seasonal solar thermal energy storage (SSTES) for a single family dwelling using TRNSYS. Sol Energy 2012;86:289–300.

[34] Hamm V, Bazargan Sabet B. Modelling of fluid flow and heat transfer to assess the geothermal potential of a flooded coal mine in Lorraine, France. Geothermics 2010;39:177–86.

[35] Ghoreishi-Madiseh SA, Hassani FP, Mohammadian A, Radziszewski PH. A transient natural convection heat transfer model for geothermal borehole heat exchangers. J Renew Sustain Energy 2013;5:043104.

[36] Ghoreishi-Madiseh SA, Sasmito AP, Hassani FP, Amiri L. Heat transfer analysis of large scale seasonal thermal energy storage for underground mine ventilation. The 7th international conference on applied energy –ICAE2015. Energy Procedia 2015;75:2093–8.

[37] Zhou Xuezhi, Xu Yujie, Zhang Xinjing, Xu Dehou, Linghu Youqiang, Guo Huan, Wang Ziyi, Chen Haisheng. Large scale underground seasonal thermal energy storage in China. J Energy Storage 2021;33:102026.

[38] Han M. Theoretical and experimental study on solar-ground coupled heat pump with seasonal storage (Master thesis), Tianjin China: Tianjin University; 2007.

[39] Yang Weibo, Zhang Yu, Wang Feng, Liu Aihua. Experimental and numerical investigations on operation characteristics of seasonal borehole underground thermal energy storage. Renew Energy 2023;217:119365.

[40] Gabrielli P, Acquilino A, Siri S, Bracco S, Sansavini G, Mazzotti M. Optimization of low-carbon multi-energy systems with seasonal geothermal energy storage: The anergy grid of ETH zurich. Energy Convers Manag: X 2020;8:100052.

[41] Lamarche L, Beauchamp B. A new contribution to the finite line-source model for geothermal boreholes. Energy Build 2007;39:188–98.

[42] Hałaj E, Pajak L, Papiernik B. Finite element modeling of geothermal source of heat pump in long-term operation. Energies 2020;13:1341.

[43] Abbas Z, Yong L, Abbas S, Chen D, Li Y, Wang RZ. Performance analysis of seasonal soil heat storage system based on numerical simulation and experimental investigation. Renew Energy 2021;178:66–78.

[44] Pokhrel S, Amiri L, Poncet S, Ghoreishi-Madiseh SA. Reduced order 1 + 3D numerical model for evaluating the performance of solar borehole thermal energy storage systems. J Energy Storage 2023;66:107503.

[45] Sáez Blázquez C, Farfán Martín A, Martín Nieto I, Gonzalez-Aguilera D. Measuring of thermal conductivities of soils and rocks to be used in the calculation of a geothermal installation. Energies 2017;10(6):795.

[46] Voronin VD, Ivanov E, Gushchin P, Fakhrullin R, Vinokurov V. Clay composites for thermal energy storage: A review. Molecules 2020;25(7):1504.

[47] Lan Y, Liu Y, Li J, Chen D, He G, Parkin IP. Natural clay-based materials for energy storage and conversion applications. Adv Sci 2021;8(11):2004036.

[48] Wang C, Liang W, Tang Z, Jia J, Liu F, Yang Y, Li A. Enhanced light-thermal conversion efficiency of mixed clay base phase change composites for thermal energy storage. Appl Clay Sci 2020;189:105535.

[49] Xu Y, Zeng Z. Experimental and numerical investigation on the effect of heat and moisture coupling migration of unsaturated lateritic clay for the soil thermal storage system. Energy Build 2022;276:112499.

[50] Yang T, Liu W, Kramer GJ, Sun Q. Seasonal thermal energy storage: A techno-economic literature review. Renew Sustain Energy Rev 2021;139:110732.

[51] Nieto IM, Carrasco García P, Sáez Blázquez C, Farfán Martín A, González-Aguilera D, Carrasco García J. Geophysical prospecting for geothermal resources in the south of the Duero Basin (Spain). Energies 2020;13(20):5397.

[52] Stewart M, Gay MC. Evaluation of transient electromagnetic soundings for deep detection of conductive fluids. Groundwater 1986;24(3):351–6.

[53] Sáez Blázquez C, Carrasco García P, Nieto IM, Maté-González MÁ, Martín AF, González-Aguilera D. Characterizing geological heterogeneities for geothermal purposes through combined geophysical prospecting methods. Remote Sens 2020;12(12):1948.

[54] Nieto IM, Carrasco García P, Sáez Blázquez C, Farfán Martín A, González-Aguilera D, Carrasco García J. Geophysical prospecting for geothermal resources in the south of the Duero Basin (Spain). Energies 2020;13(20):5397.

[55] Fitterman DV, Stewart MT. Transient electromagnetic sounding for groundwater. Geophysics 1986;51(4):995–1005.

[56] Butler DK. Implications of magnetic backgrounds for unexploded ordnance detection. J Appl Geophys 2003;54(1–2):111–25.

[57] Instituto geográfico nacional. 2023, accessed on 2023 https://centrodedescargas.cnig.es/CentroDescargas/index.jsp.

[58] Carman PC. Permeability of saturated sands, spoils and clays. J Agric Sci 1939;29:262–73. http://dx.doi.org/10.1017/S0021859600051789.

[59] Neuzil CE. Permeability of clays and shales. Annu Rev Earth Planet Sci 2019;47:247–73. http://dx.doi.org/10.1146/annurev-earth-053018-060437.

[60] Catolico N, Ge S, McCartney JS. Numerical modeling of a soil-borehole thermal energy storage system. Vadose Zone J 2016;15(1):1–17.

[61] Gabrielsson A, Bergdahl U, Moritz L. Thermal energy storage in soils at temperatures reaching 90 °C. J Solar Energy Eng 2000;122(1):3–8. http://dx.doi.org/10.1115/1.556272, (6 pages).

[62] van Meurs GAM, Hoggendorn CJ. Influence of natural convection on the heat losses for seasonal heat storage in the soil. In: Proceedings of international conference on subsurface heat storage in theory and practice, stockholm, Sweden, appendix part I. 1983, p. 475–80.

[63] van Meurs GAM. Seasonal heat storage in the soil (Ph.D. thesis), The Netherlands: Dept. of Applied Physics, University of Technology in Delft; 1985, http://resolver.tudelft.nl/uuid:723e13a9-c9f2-4748-86e6-0a558dfb70a2.

[64] Çengel YA, Ghajar AJ. Heat en mass transfer: fundamentals and applications. New York: McGraw-Hill Education; 2015.

[65] https://www.makeitfrom.com/material-properties/Acrylonitrile-Styrene-Acrylate-ASA.

[66] https://www.fluorotherm.com/technical-information/materials-overview/pvdf-properties/.

[67] https://www.fluorotherm.com/technical-information/materials-overview/pfa-properties/.

[68] Polypropylene Random Cpolymer (PPRC). Jordan J Mech Ind Eng 2008;2(4).

[69] Nikiforova T, Savytskyi M, Limam K, Bosschaerts W, Belarbi R. Methods and results of experimental researches of thermal conductivity of soils. Energy Procedia 2013;42:775–83.

[70] Abu-Hamdeh NH. Thermal properties of soil. Biosyst Eng 2003;86(1):97–102.

[71] Sáez Blázquez C, Farfán Martín A, Nieto IM, Carrasco García P, Sánchez Pérez LS, González-Aguilera D. Thermal conductivity map of the Avila region (Spain) based on thermal conductivity measurements of different rock and soil samples. Geothermics 2017;65:60–71.

[72] Anton H. Calculus with analytic geometry. 2nd ed.. New York: Wiley; 1984, p. 262–3, ISBN 100471153060.

[73] Average monthly temperature from SARAH-2 Solar Radiation DataBase, by EUMETSAT Climate Monitoring Satellite Application Facility https://re.jrc.ec.europa.eu/pvg_tools/en/tools.html.

[74] Oliveti G, Arcuri N, Ruffolo S. First experimental results from a prototype plant for the interseasonal storage of solar energy for the winter heating of buildings. Sol Energy 1998;62:281–90.

[75] Schmidt T, Mangold D, Müller-Steinhagen H. Central solar heating plants with seasonal storage in Germany. Sol Energy 2004;76:165–74.

[76] Hahne E. The ITW solar heating system: an oldtimer fully in action. Sol Energy 2000;69:469–93.

[77] Reuss M, Beuth W, Schmidt M, Schoelkopf W. Solar district heating with seasonal storage in attenkirchen. ECOSTOCK'2006. In: 10th international conference on thermal energy storage. Stockton, USA; 2006.

[78] Lundh M, Dalenbäck JO. Swedish solar heated residential area with seasonal storage in rock: initial evaluation. Renew Energy 2008;33:703–11.

[79] Fisch MN, Guigas M, Dalenbäck JO. A review of large-scale solar heating systems in Europe. Sol Energy 1998;63:355–66.

[80] Behbehani F, McCartney JS. Energy pile groups for thermal energy storage in unsaturated soils. Appl Therm Eng 2022;215:119028.